Available online at www.sciencedirect.com
SCIENCE DIRECT®
Mechanism and Machine Theory 39 (2004) 695–715
Mechanism and Machine Theory
www.elsevier.com/locate/mechmt

Dynamic tooth loads of planetary gear sets having tooth profile wear

C. Yuksel [a], A. Kahraman [b,*]

[a] The University of Toledo, Toledo, OH 43606, USA
[b] Department of Mechanical Engineering, The Ohio State University, Room 255, 650 Ackerman Road, Columbus, OH 43202, USA

Received 25 June 2003; received in revised form 12 January 2004; accepted 10 February 2004

Abstract

A computational model of a planetary gear set is employed to study the influence of surface wear on the dynamic behavior of a typical planetary gear set. The overall computational scheme combines a wear model that defines geometric description of contacting gear tooth surfaces having wear and a deformable-body dynamic model of a planetary gear set. The wear model employs a quasi-static gear contact model to compute contact pressures and Archard's wear model to determine the wear depth distributions. The worn surfaces are input into the dynamic model to quantify the impact of wear on gear tooth and mesh dynamic forces. The results on a planetary gear set having a fixed planet carrier indicates that the dynamic behavior is nonlinear due to tooth separations in its resonance regions. The results for worn gear surfaces indicate that surface wear has a significant influence in off-resonance speed ranges while its influence diminishes near resonance peaks primarily due to tooth separations.

Keywords: Planetary gear sets; Gear dynamics; Gear wear

1. Introduction

Planetary gear sets, also known as Epicyclic gear drives, are commonly used in a large number of automotive, aerospace and industrial applications. They posses numerous advantages over parallel-axis gear trains including compactness of design, availability of multiple speed reduction ratios, and

* Corresponding author. Tel.: +1-614-292-4678; fax: +1-614-292-3163/3603.
E-mail address: kahraman.1@osu.edu (A. Kahraman).

0094-114X/$ - see front matter
doi:10.1016/j.mechmachtheory.2004.03.001

less demanding bearing requirements. Most common examples of planetary gear sets can be found in automatic transmissions, gas turbines, jet engines, and helicopter drive trains. A typical simple planetary gear set consists of a sun gear, a ring gear and a number of identical planet gears (typically 3–6) meshing both with the sun and ring gears. A common carrier holds the planets in place.

Dynamic analysis of planetary gears is essential for eliminating noise and vibration problems of the products they are used in. The dynamic forces at the sun-planet and ring-planet meshes are the main sources of such problems. Although planetary gear sets have generally more favorable noise and vibration characteristics compared to parallel-axis gear systems, planetary gear set noise still remains to be a major problem. The dynamic gear mesh loads that are much larger than the static loads are transmitted to the supporting structures, in most cases, increasing gear noise. Larger dynamic loads also shorten the fatigue life of the components of the planetary gear set including gears and bearings.

Surface wear is considered one of the major failure modes in gear systems. In case of planetary gear sets, experimental data has shown that especially the sun gear meshes might experience significant surface wear when run under typical operating conditions [1]. While wear is a function of a large number of parameters, sliding distance and contact pressure were shown to be most significant parameters influencing gear wear [1]. Wear of tooth profiles results in a unique surface geometry that alters the gear mesh excitations in the form of kinematic motion errors, enhancing the dynamic effects.

Modeling of planetary gear set dynamics received significant attention for the last 30 years. A number of studies proposed lumped-parameter models to predict free and forced vibration characteristics of planetary gear sets [2–9]. These models assumed rigid gear wheels, connected to each other by springs representing the flexibility of the meshing teeth. In these studies (except [6]), nonlinear effects due to gear backlash and time-varying parameters due to gear mesh stiffness fluctuations were neglected. The corresponding Eigen value solution of the linear equations of motion resulted in natural modes. Modal summation technique was typically used to find the forced response due to external gear mesh displacement excitations defined to represent motion transmission errors. These lumped-parameter models vary in degrees of freedom included, from purely torsional models [2–4,9] to two [5,6,8] or three-dimensional transverse-torsional models [7]. While these models served well in describing the dynamic behavior of planetary gear sets qualitatively, they lacked certain critical features. First, the gear mesh models were quite simplistic with a critical assumption that complex gear mesh contact interaction can be represented by a simple model formed by a linear spring and a damper. These models demand that the values of the gear mesh stiffness and damping, as well as the kinematic motion transmission error excitation, must be known in advance. It is also assumed that these parameter values determined quasi-statically remain unchanged under dynamic conditions. In addition, gear rim deflections and Hertzian contact deformations are also neglected. Another group of recent models [10,11] used more sophisticated finite element-based gear contact mechanics models. These computational models address all of the shortcomings of the lumped-parameter models since the gear mesh conditions are modeled as individual nonlinear contact problems. The need for externally defined gear mesh parameters is eliminated with these models. In addition, rim deflection and spline support conditions are modeled accurately [12]. These models are also capable of including the influence of the tooth profile variations in the form of intentional profile modifications, manufacturing errors or wear on the dynamic behavior of the system.

The study of wear of gear contact is becoming one of the emerging areas in gear technology. A number of recent gear wear modeling efforts [1,13–16] form a solid foundation for more accurate, larger system analyses. All of these models use Archard's wear model [17] in conjunction with a gear contact model and relative sliding calculations. These studies focused on prediction of wear of either spur [13,14] or helical [1,15,16] gear pairs in a parallel-axis configuration. The tooth contact pressures were computed in these models using either simplified Hertzian contact [14–16] or boundary element [1] formulations under quasi-static conditions. Sliding distance calculations were carried out kinematically by using the involute geometry and Archard's wear model was used with an empirical wear coefficient to compute the surface wear depth distribution.

A number of studies investigated the influence of wear on gear dynamics response [18–20]. Among them, Kuang and Lin [18] simulated the tooth profile wear process by the model proposed by Ref. [14], and predicted the variations of the dynamic loads and the corresponding frequency spectra as a function of wear for a single spur gear pair. Wojnarowski and Onishchenko [20] performed analytical and experimental investigations of the influence of the tooth deformation and wear on spur gear dynamics. They stated that the change in the profiles of the teeth due to wear must be taken into account when dealing with the durability of the gear transmissions as well. These previous models considered surface wear effects for only a single spur gear pair, avoiding multi-mesh gear systems such as the planetary gear sets. They focused on only external gears and used lumped-parameter dynamic models excluding nonlinear and time-varying effects.

1.1. Objectives and scope

As none of the previous studies on planetary gear set dynamics took into account the effect of wear, this study is intended to describe to the influence of gear tooth surface wear on dynamic behavior of planetary gears. A deformable-body dynamic model similar to the one proposed earlier [11] will be used to investigate the influence of tooth surface wear on the dynamic behavior of planetary gear sets. The main objective here is to quantify the influence of surface wear on dynamic behavior of planetary gear sets. A planetary gear set formed by spur gears will be considered. A wear prediction model will be proposed to predict the gear surface wear distribution under quasi-static conditions. Different amounts of wear depths will then be introduced in the dynamic model to quantify the differences in dynamic behavior from the baseline behavior representing a gear set having no wear. Several complex dynamic phenomena exhibited by the planetary gear set including nonlinear behavior such as jump discontinuities and tooth separations will be demonstrated. The influence of surface wear on such behavior will also be described.

2. Computational model

This study relies on two previously developed models for investigation of the effect of surface wear on the dynamics of planetary systems. First, a wear model developed by Bajpai et al. [1] will be used to determine the tooth surface wear profiles after different wear cycles. This model uses quasi-static finite elements-based gear contact model for prediction of the gear contact pressures and employs Archard's wear model to predict wear of contacting tooth surfaces. Predicted tooth surface wear will then be applied to a deformable-body planetary gear dynamic model similar to

the one proposed by Kahraman et al. [11] to quantify the impact of gear surface wear on the dynamic behavior of planetary gear sets.

2.1. Wear prediction model

Archard's wear equation [17] can be expressed for a local point on one of the contacting gear surfaces as

$$h = \int_0^s kP\,\mathrm{d}s \tag{1}$$

where k is an experimentally determined wear coefficient, h is the wear depth accumulated, P is the contact pressure, and s is the sliding distance between the mating surfaces at the point of interest. Here, all the parameters other than the contact pressure and sliding distance are accounted for by k. These include many material, heat treatment, surface roughness and lubrication related parameters. While the wear model can be improved by describing additional parameters explicitly in Eq. (1), it was shown to work sufficiently well for engineering purposes [1].

The flowchart of the overall wear prediction model is shown in Fig. 1 [1]. The initial geometric description of the gear tooth surfaces serves as the initial state for the wear prediction and each gear tooth contact surface is denoted by $(G_{ij}^{\kappa})^p$ and $(G_{ij}^{\kappa})^g$ where p and g represent the driving and the driven gears. Here, G_{ij} is the deviation of a tooth surface point ij from the perfect involute surface, and κ indicates the number of geometry updates done so far in analysis with $\kappa = 0$ meaning that the gear surfaces are the initial unworn ones. A fixed surface grid is defined in the active surface of the tooth of interest (for both gears) by defining I equally spaced grid lines ($i = 1, 2, \ldots, I$) in the involute direction and J equally spaced grid lines ($j = 1, 2, \ldots, J$) in the face width direction.

A commercial quasi-static deformable-body contact mechanics model [21] is employed here to predict the instantaneous contact pressure distributions at discrete rotational positions $r \in [0, R]$ where the amount of gear rotation accomplished between $r = 0$ and $r = R$ covers a complete wear cycle of the tooth of interest. In other words, at $r = 0$, the tooth of interest on gear p initiates contact near its root with a tooth of gear g. The contact line moves upward on this tooth leaving the tooth at its tip at $r = R$. The contact mechanics model which applies a FE model in conjunction with a surface integral formulation [21] gives the contact pressures $(P_{ij}^{\kappa})_r^{p,g}$ of point ij of the teeth of p or g at a given rotational position r.

Next, the sliding distance $(s_{ij}^{\kappa})_{r\to r+1}^{p,g}$ is defined as the distance by which a point represented by node ij on one gear slides with respect to its corresponding point on the mating gear as gears rotate from position r to position $r + 1$. The sliding distance calculations must be carried out only for the nodes with nonzero $(P_{ij}^{\kappa})_r^{p,g}$ for at least two consecutive rotational positions and must be continued as r is increased until $(P_{ij}^{\kappa})_r^{p,g}$ becomes zero again. Assume that the leading edge of the contact zone reaches a node ij on gear p at $r = m$, and at this position, it is in contact with a point a on gear g. In other words, their position vectors are equal at this instant, $(\mathbf{X}_a)_m^g = (\mathbf{X}_{ij})_m^p$. When the gears are rotated to the next position $r = m + 1$, these two points are no longer in contact and the distance between them represents the sliding distance occurred between positions $r = m$ and $r = m + 1$, i.e.

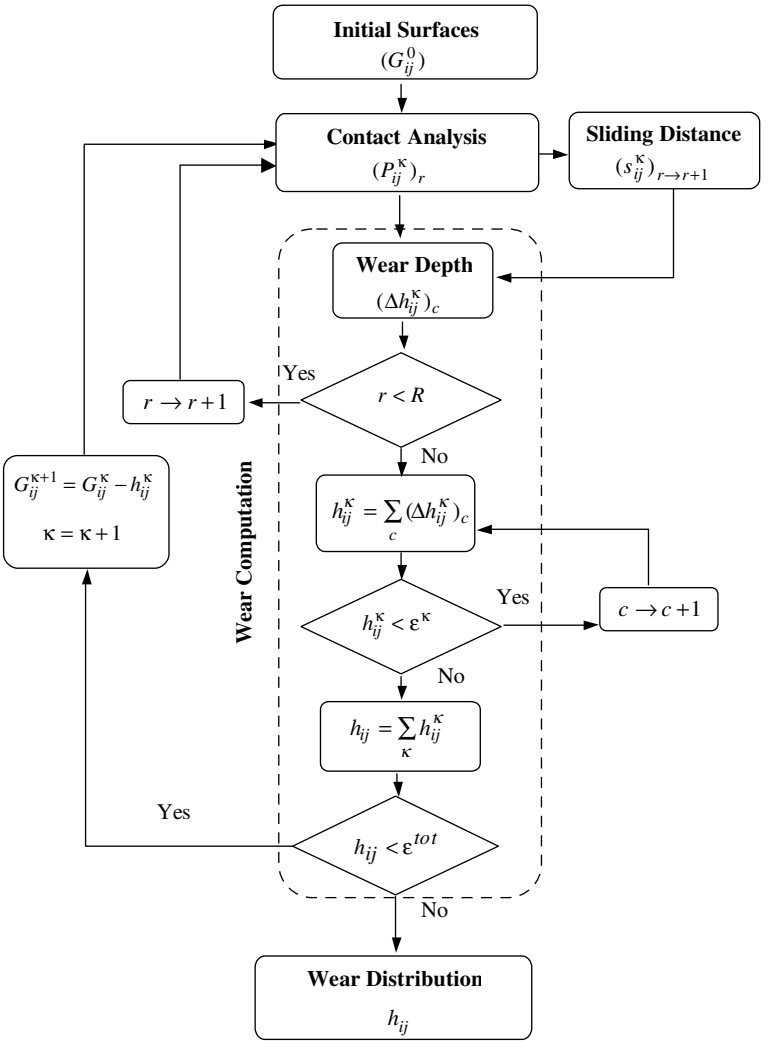

Fig. 1. Flowchart of the iterative tooth wear prediction procedure [1] consisting of models for gear contact, sliding distance and wear computations.

$$(s_{ij}^{\kappa})_{m\to m+1}^{p} = \|(\mathbf{X}_a)_{m+1}^{g} - (\mathbf{X}_{ij})_{m+1}^{p}\| \tag{2}$$

If the contact zone leaves the same point ij after position $r = t$, the sliding distance experienced by nodal point ij of gear p as gears rotate from position r to $r+1$ is given in general terms as [1]

$$(s_{ij}^{\kappa})_{r\to r+1}^{p} = \begin{cases} \left| \|(\mathbf{X}_a)_{r+1}^{g} - (\mathbf{X}_{ij})_{r+1}^{p}\| - \sum_{q=m}^{r} (s_{ij}^{\kappa})_{q-1\to q}^{p} \right|, & m \leqslant r \leqslant t \\ 0, \quad 0 \leqslant r \leqslant m \text{ or } t < r < R \end{cases} \tag{3}$$

This procedure is repeated for the points of gear g as well. With $(P_{ij}^{\kappa})_r^{p,g}$ and $(s_{ij}^{\kappa})_{r\to r+1}^{p,g}$ $(r \in [0, R])$ are known, the wear occurred at each node between positions r and $r+1$ is calculated from Eq. (1) as

$$(\delta h_{ij}^{\kappa})_{r\to r+1}^{p,g} = \frac{1}{2} k^{p,g} (s_{ij}^{\kappa})_{r\to r+1}^{p,g} \left\{ (P_{ij}^{\kappa})_{r}^{p,g} + (P_{ij}^{\kappa})_{r+1}^{p,g} \right\} \tag{4}$$

Thus, the total wear accumulated at node ij during one complete wear cycle becomes

$$(\Delta h_{ij}^{\kappa})^{p,g} = \sum_{r=0}^{R} (\delta h_{ij}^{\kappa})_{r\to r+1}^{p,g} \tag{5}$$

Accumulated wear depth is obtained by adding wear depth for many cycles until it reaches ε^{κ}. Here, ε^{κ} is a predetermined threshold value that represents a certain amount of change on $(G_{ij}^{\kappa-1})^{p,g}$ to warrant a new contact analysis to update the pressures corresponding to the new worn geometries $(G_{ij}^{\kappa})^{p,g}$. When the maximum wear depth reaches ε^{κ} at any point on the tooth surface since the last geometry update, the new worn geometry is fed into the contact mechanic model for an update of $(P_{ij}^{\kappa})_{r}^{p,g}$. The wear amount at nodes ij of gears p and g accumulated after the κth pressure update can be written as

$$(h_{ij}^{\kappa})^{p,g} = \sum_{c=1}^{C^{\kappa}} (\Delta h_{ij}^{\kappa})_{c}^{p,g} \tag{6}$$

where C^{κ} is the number of wear cycles required to reach the wear threshold ε^{κ}. After carrying out the iterations until κth geometry update when a point on either gear surface reaches the maximum allowable wear value of ε^{tot}, the total wear depth distribution at node ij just before the κth update is given by

$$h_{ij}^{p,g} = \sum_{\kappa=1}^{K} (h_{ij}^{\kappa})^{p,g} \tag{7}$$

2.2. Deformable-body dynamics model

Worn surface profiles $(G_{ij}^{\kappa})^{p,g}$ predicted by the wear model are used in a dynamic model to quantify the changes in dynamic behavior. A commercial gear contact mechanics software package [22] is used to develop the dynamic model of the planetary gear set. The model uses finite element (FE) method to compute relative deformations and stresses for points away from the contact zones and semi analytical techniques for the points within the contact zones, is employed [22]. The semi analytical FE approach does not require a highly refined mesh at the contacting tooth surfaces, reducing the computational effort while conventional FE models require a refined mesh at gear tooth region, limiting the model to static analysis only. Therefore, the model used here allows a more accurate and comprehensive study of planetary gear dynamics than the conventional FE models [11]. The gears have complex shapes that can be best modeled by the FE method. The tooth surfaces are modeled by a large number of coordinate nodes, representing the involute shape and surface modifications making it possible to incorporate worn profiles $(G_{ij}^{\kappa})^{p,g}$. The width of the contact zone in typical gear applications is two orders of magnitude smaller than the dimensions of the gear teeth themselves, requiring a very fine mesh inside the contact zone. The location of the contact zone changes as the gears enter and exit the mesh. When conventional FE models are used, besides having an extremely refined mesh, re-meshing is necessary for every

contact position. The model used here avoids this problem since deformations near or at the contact zone predicted by using a semi-analytical formulation are matched with the deformations away from the contact predicted by using FE method.

The model attaches a reference frame to each individual component and the finite element computations are done for each individual component separately. The mesh stiffness and mesh contact forces, comprising the dynamic excitation for the system, are evaluated internally at each time step [22]. Contact conditions are handled as essentially linear inequality constraints whose convergence is ensured by a revised Simplex solver.

A contact analysis determines the contact stresses and deformations of the gears at each time step. The elastic deformations of the gears are much smaller and must be superposed on the rigid body motions. By choosing a gear coordinate frame that follows the rigid body motion, the FE displacement vector $\mathbf{x}_{fi}$ for gear i can be represented by a linear system of differential equations [10,11]

$$\mathbf{M}_{ffi}\ddot{\mathbf{x}}_{fi} + \mathbf{C}_{ffi}\dot{\mathbf{x}}_{fi} + \mathbf{K}_{ffi}\mathbf{x}_{fi} = \mathbf{f}_{fi} \tag{8}$$

where $\mathbf{f}_{fi}$ is the vector of external loads. Rayleigh's damping model is used here in the form $\mathbf{C}_{ffi} = \mu\mathbf{M}_{ffi} + \eta\mathbf{K}_{ffi}$ where μ and η are constant coefficients. Representing the rigid body motions of the reference frame by $\mathbf{x}_{ir}$ and combining it with Eq. (8) results in

$$\begin{bmatrix} \mathbf{M}_{ffi} & \mathbf{M}_{fri} \\ \mathbf{M}_{rfi} & \mathbf{M}_{rri} \end{bmatrix} \begin{Bmatrix} \ddot{\mathbf{x}}_{fi} \\ \ddot{\mathbf{x}}_{ri} \end{Bmatrix} + \begin{bmatrix} \mathbf{C}_{ffi} & \mathbf{C}_{fri} \\ \mathbf{C}_{rfi} & \mathbf{C}_{rri} \end{bmatrix} \begin{Bmatrix} \dot{\mathbf{x}}_{fi} \\ \dot{\mathbf{x}}_{ri} \end{Bmatrix} + \begin{bmatrix} \mathbf{K}_{ffi} & \mathbf{K}_{fri} \\ \mathbf{K}_{rfi} & \mathbf{K}_{rri} \end{bmatrix} \begin{Bmatrix} \mathbf{x}_{fi} \\ \mathbf{x}_{ri} \end{Bmatrix} = \begin{Bmatrix} \mathbf{f}_{fi} \\ \mathbf{f}_{ri} \end{Bmatrix}. \tag{9}$$

The equations for each gear are assembled into the entire planetary gear system to obtain the overall matrix equation of motion

$$\mathbf{M}\ddot{\mathbf{x}} + \mathbf{C}\dot{\mathbf{x}} + \mathbf{K}\mathbf{x} = \mathbf{F} \tag{10}$$

For the solution of the above equation, the contact mechanics model [22] employs a time-discretization scheme based on Newmark method as used successfully in previous studies [10,11].

3. Results and discussion

An example spur-type planetary system representative of typical gear sets in automatic transmission systems is considered here. Design parameters of the example system are listed in Table 1 and dynamic model is shown in Fig. 2. The sun gear is the input, the internal gear is the output, and the carrier is held stationary. A constant torque of 25 Nm/mm face width (FW) is applied to the input member. The system has four equally spaced planets that are not allowed to float radially. In order to avoid added complexity of ring gear bending modes [11], the outside diameter of the internal gear is chosen as rigid throughout this study while radial planet bearing flexibilities are included.

Dynamic analysis of the model shown in Fig. 2 took a significant computational time. The simulation must be carried out for a reasonably long period to surpass the transient region. For each analysis, first a speed ramp up was simulated for a complete input revolution to pass through the transients, followed by a more refined analysis at the desired speed to cover two complete input revolutions. The steady state response is extracted from the last stage of the analysis. When

Table 1
Design parameters of the example system (all dimensions are in mm unless specified)

	Sun	Planet	Ring
Number of teeth	34	18	70
Module	1.5	1.5	1.5
Pressure angle, degrees	21.3	21.3	21.3
Circular tooth thickness	1.895	2.585	1.884
Hob tip radius	0.2	0.2	–
Fillet radius	–	–	0.5
Outer radius	26.37	15.25	58.95
Root radius	23.00	11.875	55.00
Minor radius	–	–	51.725
Inner radius	12.88	5.94	–
Face width	30	30	30

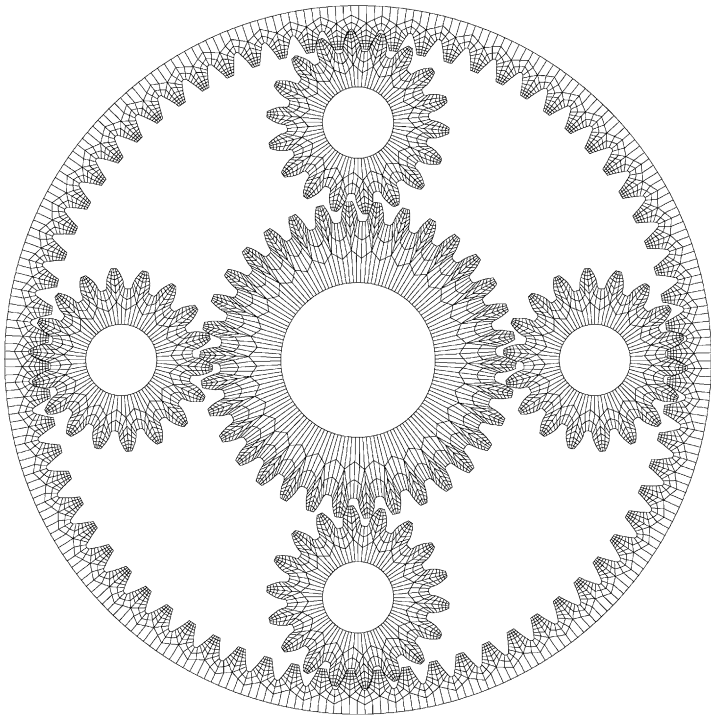

Fig. 2. Two-dimensional deformable-body dynamic model of the example planetary gear set having a stationary carrier.

the input speed is increased by a small increment, as it is the case in an actual speed sweep, the last point of the steady state motion from the previous speed increment was considered as the initial condition followed by a rapid ramp-up and a refined steady state simulation.

Dynamic analyses were performed within an input speed range up to $\Omega_{in} = 15,000$ rpm, with a speed increment between 50 and 250 rpm. In each analysis, individual tooth loads at the sun and

ring gear meshes of the planet gears were considered the output parameters. The time increment is adjusted at each analysis such that there are nearly 120 data points per tooth mesh cycle that was found to be a sufficient resolution to capture high frequency dynamic effects on tooth loads. Total gear mesh force time histories were obtained by adding all tooth forces at a given mesh and the corresponding frequency spectrum was obtained by using a fast Fourier transform (FFT) routine.

In predicting the wear depth, a wear coefficient value of $k = 10^{-18}$ m^2/N was used in this analysis. This value was determined experimentally by Bajpai et al. [1] using a similar automatic transmission final drive planetary gear set formed by case carburized shaved external gears and shaped internal gears. Bajpai, et.al. also pointed out that the wear at the ring-planet meshes is simply negligible compared to those measured at the sun-planet meshes. In the power flow configuration considered, a sun gear tooth that mates with four planets will experience four wear cycles per input revolution, while a ring tooth goes through only $4(Z_s/Z_r) = 4(34/70) = 1.94$ wear cycles for the example system. Therefore, given this kinematic condition and previous experimental observations [1], wear at the ring-planet mesh was neglected in this study all together for the sake of simplicity.

At the beginning, the sun and the planet gears are assumed to have perfect involute profiles with no modifications, i.e. $(G_{ij}^0)^{p,g} = 0$ in Fig. 1. The initial contact pressures $(P_{ij}^0)_r^{p,g}$ were predicted by using the contact mechanics model of Fig. 3 [24]. Here p and g denote the sun and planet gear, respectively. The contact analysis was carried out at $R = 200$ rotational positions covering a complete wear cycle through a total of 20° of rotation. The fixed tooth surface grid is defined by a total of 10,000 points with $I = 50$ and $J = 200$. Using the $(P_{ij}^0)_r^{p,g}$ values, the wear analysis is

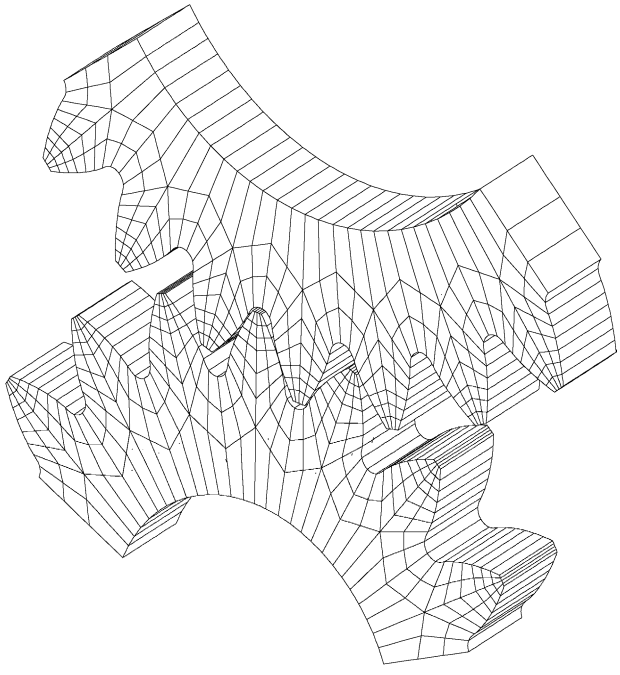

Fig. 3. A three-dimensional quasi-static contact mechanics model of the sun-planet pair of the example planetary gear set.

continued until the maximum wear depth at any of the grid points reaches the threshold value of $\varepsilon^{\kappa} = 2.5$ μm. At that point, worn surface geometries $(G_{ij}^{1})^{p,g}$ are used to update the pressure values by using the contact model to obtain $(P_{ij}^{1})_{r}^{p,g}$. This is followed by another wear simulation until the change in the worn geometry again reaches $\varepsilon^{\kappa} = 2.5$ μm to warrant another pressure update. This iterative loop is repeated six times ($\kappa = 1$–6). The wear analysis is terminated when the total cumulative wear of any point on surfaces of either gear reaches ε^{tot} value of nearly 15 μm.

Fig. 4 shows the distribution of wear depth at various κ in the mid-plane of the gears as a function of gear roll angles. Only the wear amounts in this mid-plane are shown since the wear profiles remain uniform along the face width of gears. It is evident from Fig. 4(a) that wear along the pitch line of the sun gear at roll angles of 22.3° is minimal since the relative sliding at pitch point is theoretically zero. The same is thru for the planet gear as well. Maximum wear on sun gear occurs in the dedendum region, below the pitch line. Wear depth goes to zero at the tip since

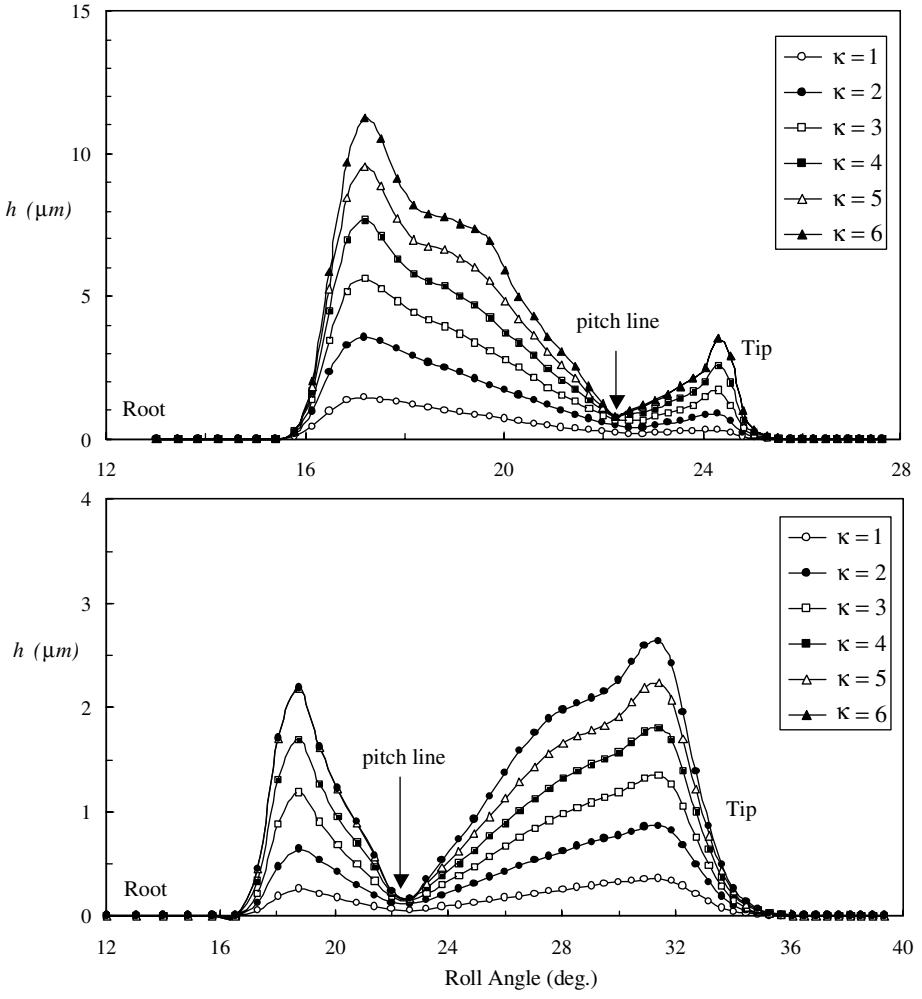

Fig. 4. Wear distribution in the mid-plane of (a) sun gear and (b) planet gear as a function of roll angle, $\kappa = 1$–6.

both the sun gear and planets have tip chamfer. A similar wear pattern is observed for the mating planet gear, except the addendum wear is more significant and the maximum wear depth of the planet gear tooth is considerably smaller than those of the sun gear. One reason for this is that for each complete rotation (again for the particular power flow considered here with a four planet system), a tooth on sun goes through four wear cycles while a planet tooth has only $Z_s/Z_p = 34/18 = 1.89$ wear cycles.

3.1. Baseline dynamic response

A planetary gear set having unworn involute surfaces $(G_{ij}^0)^{p,g}$ forms the baseline for the dynamic behavior. In this study, the dynamic response of the planetary system will be described in terms of dynamic tooth and mesh loads acting on the gears. Dynamic mesh loads are of special interest since they correlate to both fatigue and noise behavior of the gear set. The dynamic model used here [22] has the post-processing capability to compute the individual tooth forces along the line of action from the distributed contact pressures. Define $F_s^{(t)}$ and $F_r^{(t)}$ as sun and ring tooth forces where superscript t denotes tooth and the subscripts s and r denote the sun and ring gears, respectively. Both $F_s^{(t)}$ and $F_r^{(t)}$ are time dependent and are given per mm FW.

Fig. 5(a1) and (b1) illustrate $F_s^{(t)}$ and $F_r^{(t)}$ at $\Omega_{\text{in}} = 2000$ rpm for three complete mesh cycles. In Fig. 5(a1), focusing on the middle mesh cycle, the mesh cycle starts with one tooth (i) carrying the entire mesh load. The next tooth $(i+1)$ starts sharing some of the load with tooth (i) for a short period before tooth (i) moves out of the mesh, leaving tooth $(i+1)$ to carry the entire mesh force. This behavior is repeated for each mesh cycle. About 1/5 of the mesh cycle has two teeth in contact and the rest has only one tooth in contact. In Fig. 5(b1), on the other hand, double tooth contact is maintained for the entire mesh cycle except a very small period in the middle of the mesh cycle when there is only one tooth contact. This difference is mostly because the ring gear meshes have larger involute contact ratios allowing more teeth to share the mesh load.

Total sun/planet and ring/planet mesh forces $F_{s/p}^{(m)}$ and $F_{r/p}^{(m)}$ are obtained by adding the tooth force time histories at a given mesh cycle i as $F_{j/p}^{(m)}(t) = F_{\text{j}}^{(t_{i-1})}(t) + F_j^{(t_i)}(t) + F_j^{(t_{i+1})}(t)$ where $j = s, r$. Fig. 5(a2) and (b2) show $F_{s/p}^{(m)}$ and $F_{r/p}^{(m)}$ as a function of mesh cycles, respectively. As both $F_{s/p}^{(m)}$ and $F_{r/p}^{(m)}$ are periodically time varying functions, a FFT analysis results in line spectra as shown in Fig. 5(a3) and (b3). Here, the horizontal frequency axis is normalized using the gear mesh frequency $f_m = Z_s\Omega_{\text{in}}/60$ in Hz where Ω_{in} is given in rpm, reducing them to order spectra.

Fig. 6 shows $F_{s/p}^{(m)}$ at four different Ω_{in} values to illustrate that $F_{s/p}^{(m)}$ amplitudes change significantly with Ω_{in}, which is also true for the ring gear meshes. Given the order spectra of $F_{j/p}^{(m)}$ at a given Ω_{in}, the root-mean-square (rms) value of $F_{j/p}^{(m)}$ $(j = s, r)$ can be defined as $F_{j/p}^{(\text{rms})} = [\sum_{i=1}^{q}(F_{j/p}^{(i)})^2]^{1/2}$ where $F_{j/p}^{(i)}$ is the ith harmonic amplitude. Here $q = 6$ was found sufficient.

In Fig. 7, $F_{s/p}^{(\text{rms})}$ and $F_{r/p}^{(\text{rms})}$ forced response curves of the example baseline system (no wear and no modifications) are shown at an input torque value of 25 Nm/mm FW. Also displayed is a second scale for the horizontal axis showing the corresponding f_m values in Hz. This range of Ω_{in} covers most aerospace and automotive applications. Fig. 7 exhibits several resonance peaks at which the dynamic loads are significantly higher than the corresponding static loads. Five such peaks were identified in both figures. Examining the variation of individual harmonic components of $F_{s/p}^{(m)}$ and $F_{r/p}^{(m)}$ with Ω_{in}, it is found that the first harmonic defines only the quasi-static

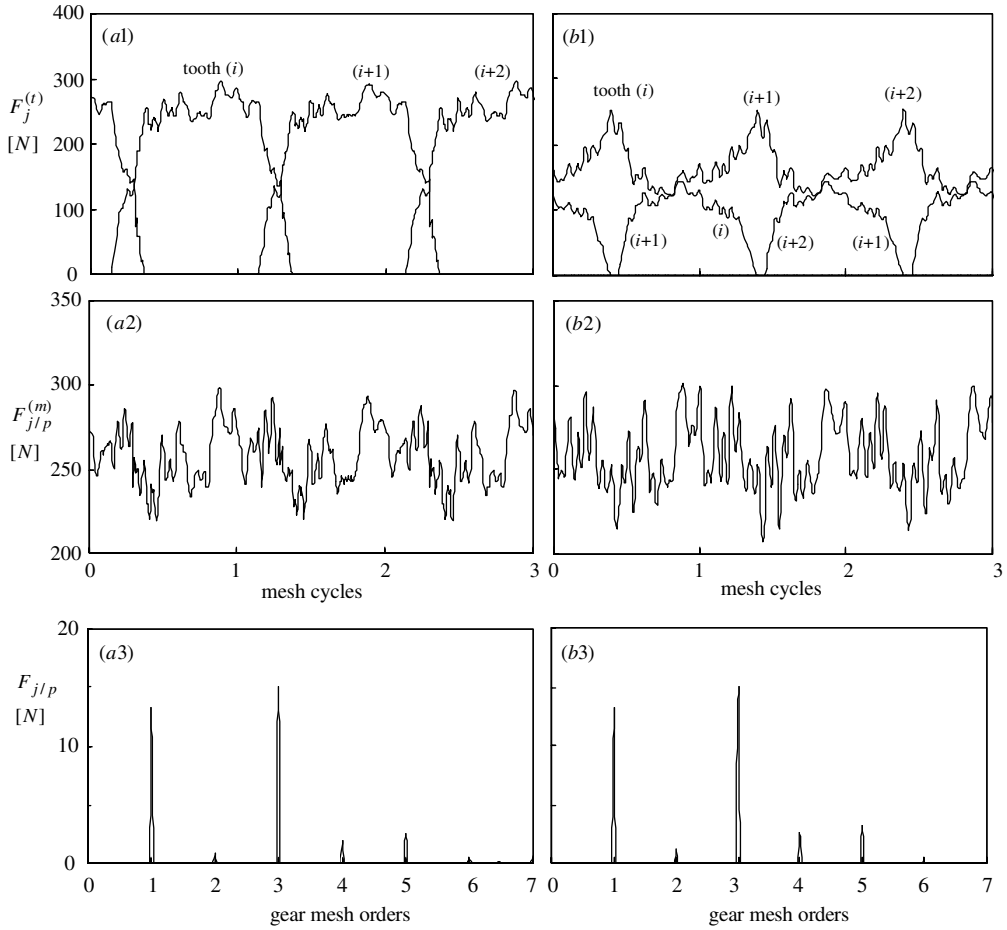

Fig. 5. Tooth forces $F_j^{(t)}$, mesh forces $F_{j/p}^{(m)}$, and order spectra of $F_{j/p}^{(m)}$ at $\Omega_{in} = 2000$ rpm; (a1)–(a3) sun gear ($j = s$) and (b1)–(b3) ring gear ($j = r$).

component of the response and it does not contribute to any of the resonance peaks. The second gear mesh harmonic component dictates the resonance peak around $\Omega_{in} = 8500$ rpm. Similarly, the third harmonic controls the peak near $\Omega_{in} = 13,000$ rpm and the fourth harmonic defines the peaks near $\Omega_{in} = 4200$ and 10,750 rpm. While such behavior might look complex, it can be described with the help of a lumped parameter dynamic model [4,7,9] and the planet-phasing formulations proposed in earlier studies [7,23]. Since the ring gear rim is not allowed to deflect and sun and planet gear rims are also relatively rigid, the purely torsional model of proposed in reference [4] should be sufficiently accurate to define the natural frequencies and the mode shapes, provided that the system parameters such as gear inertias and average gear mesh stiffness can be estimated accurately with the help of the deformable-body model [21]. This model resulted in natural frequencies of $f_1 = 0$, $f_2 = 9895$ Hz, $f_3 = f_4 = f_5 = 20,800$ Hz and $f_6 = 23,225$ Hz. It is also noted that mode shapes corresponding to f_2 and f_6 are "in-phase" while the modes corresponding to f_3–f_5 are "sequentially-phased" [4,7]. Mathematically, if the displacement vector is

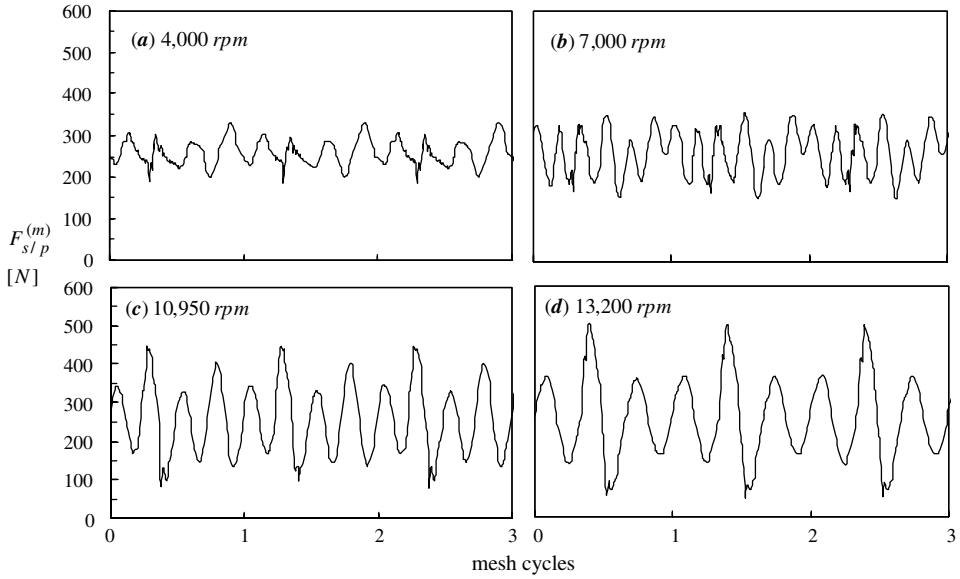

Fig. 6. $F_{s/p}^{(m)}$ time histories at different Ω_{in} values.

defined as $\Theta = [\theta_s, \theta_r, \theta_{p1}, \theta_{p2}, \theta_{p3}, \theta_{p4}]^{\text{T}}$, the shape of in-phase modes are $\Phi_{2,6} = [s, r, p, p, p, p]^{\text{T}}$ and those of the sequentially phased modes are $\Phi_{3-5} = [0, 0, p_1, p_2, p_3, p_4]^{\text{T}}$ such that $\sum_{i=1}^{4} p_i = 0$ [4,7].

It was stated earlier [7,23] that the meshes of the sun gear and the ring gear with the planets have similar phasing conditions. Specifically, for a system with equally spaced planets, the ith harmonic of any excitations originated at the meshes of the sun gear with planets will be in phase if $iZ_s/n =$ integer and sequentially phased if $iZ_s/n \neq$ integer. Similarly, the ith harmonic of any excitations originated at the meshes of the ring gear with planets are in phase if $iZ_r/n =$ integer and sequentially phased if $iZ_r/n \neq$ integer. Here Z_s and Z_r are the number of teeth of the sun and ring gears and n is the number of planets. For the example system having $Z_s = 34$ and $Z_r = 70$ and $n = 4$, $iZ_s/n =$ integer if $i =$ even and $iZ_s/n =$ non-integer if $i =$ odd suggesting that even harmonics of sun-planet mesh excitations are in phase and odd harmonics are sequentially phased. The same is true for the ring gear meshes as well. It was also shown [23] that an in-phase mode could only be excited by the ith harmonic components of gear mesh excitations if these harmonic components are in phase. Likewise, sequentially phased modes can be excited by sequentially phased ith harmonics of the excitations. Accordingly, in-phase modes at frequencies f_2 and f_6 can be excited only by the even harmonics ($i =$ even) when $f_2 \approx if_m$ or $f_6 \approx if_m$. In addition, sequentially phased modes at $f_3 = f_4 = f_5$ can be excited by the odd harmonics ($i =$ odd) when $f_3 \approx if_m$. Going back to Fig. 7, the first five resonance peaks can be stated to correspond to the resonance frequencies of $f_2 \approx 4f_m$, $f_6 \approx 6f_m$, $f_2 \approx 2f_m$, $f_6 \approx 4f_m$ and $f_3 \approx 3f_m$.

One other feature of the forced responses shown in Fig. 7 is that the amplitude curves are not continuous. In both figures, sudden changes (jumps) in amplitude are observed (shown by arrows) near resonance peaks of $f_2 \approx 4f_m$, $f_2 \approx 2f_m$, $f_6 \approx 4f_m$ and $f_3 \approx 3f_m$. In addition, the amplitudes near $f_2 \approx 2f_m$ are different depending on whether the speed is increased or decreased. There are

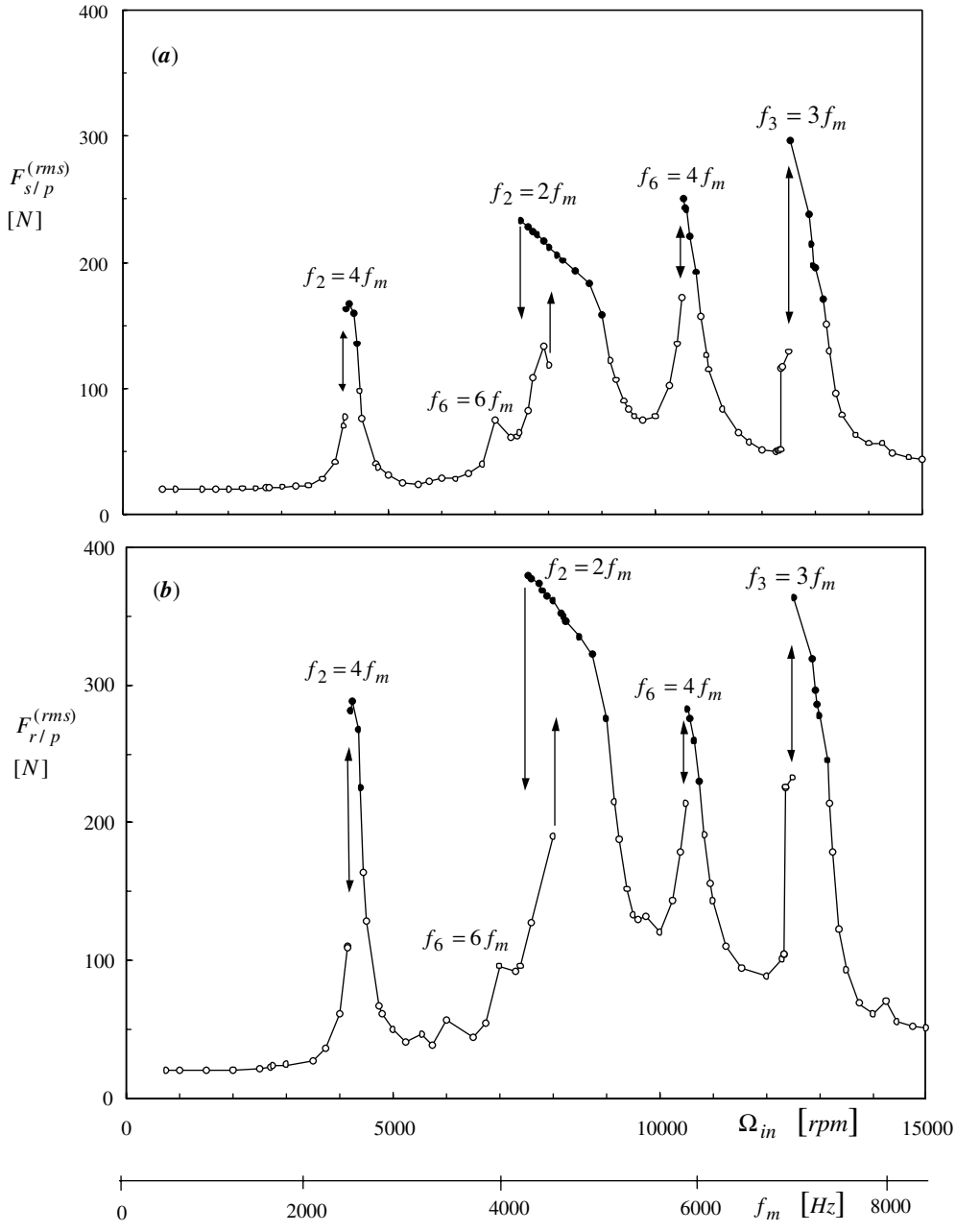

Fig. 7. (a) $F_{s/p}^{(\mathrm{rms})}$ and (b) $F_{r/p}^{(\mathrm{rms})}$ as a function of Ω_{in} and gear mesh frequency f_m at $T_{\mathrm{in}} = 25$ Nm/mm FW. (○) No tooth separation, (●) tooth separations.

two different stable motions within the speed range of $\Omega_{\mathrm{in}} \in [7475, 8000]$ rpm. When the speed is increased from $\Omega_{\mathrm{in}} = 8000$ to the next speed increment of $\Omega_{\mathrm{in}} = 8150$ rpm, $F_{s/p}^{(rms)}$ suddenly jumps up from 119 to 206 N/mm FW. Similarly, when Ω_{in} is reduced from $\Omega_{\mathrm{in}} = 8150$ rpm, $F_{s/p}^{(m)}$ con-

tinues to increase until $\Omega_{in} = 7450$ rpm when $F_{s/p}^{(rms)}$ jumps down suddenly from 233 to 65 N/mm FW. Such softening type nonlinear behavior was predicted and shown to exist experimentally [24] for single spur gear pairs. It was demonstrated that, near the resonance peak, dynamic force amplitudes can exceed the static (mean) force transmitted by the gear mesh, causing separation of teeth during a portion of the gear mesh cycle, effectively changing the gear mesh stiffness in a softening manner. In order to check whether any tooth separations take place here as well, tooth force time histories $F_{r/p}^{(m)}$ corresponding to upper branch solutions at $\Omega_{in} = 7525$, 8500 and 9000 rpm are shown in Fig. 8. In Fig. 8(a) at $\Omega_{in} = 9000$ rpm, $F_{r/p}^{(m)}$ is zero for a small duration in each mesh cycles, indicating that about 7% of each mesh cycle is when the teeth of planet-ring meshes are separated (not in contact). This phenomenon is more obvious as one move to the left on the upper branch towards the jump-down frequency. For instance, tooth separations take about 29%

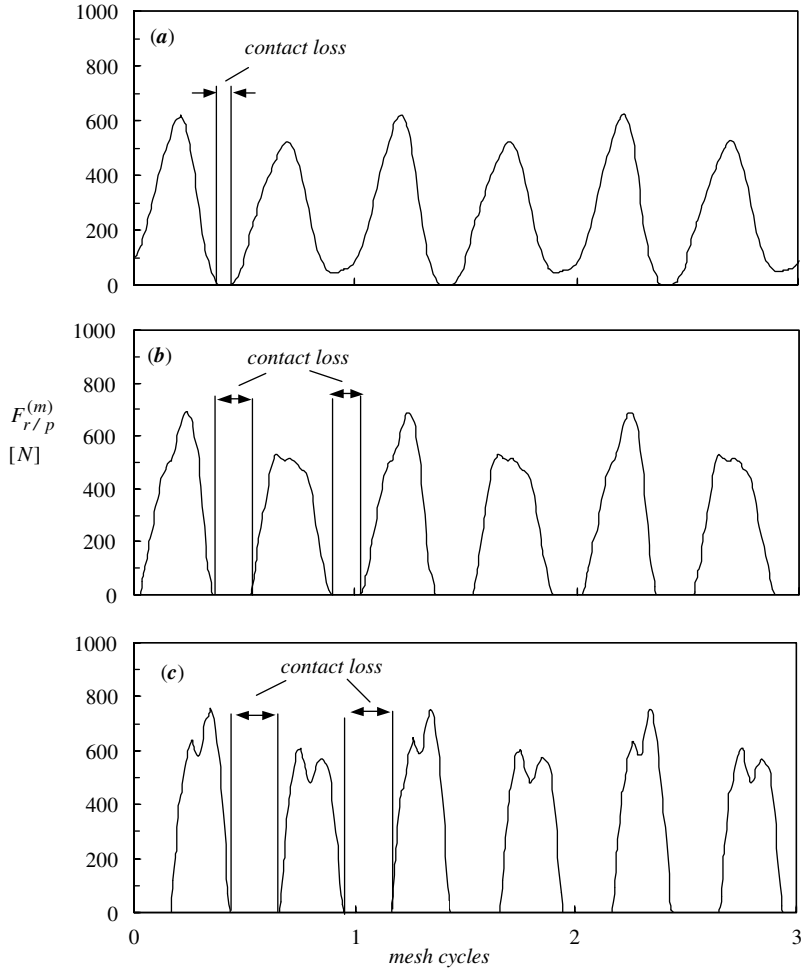

Fig. 8. Illustration of tooth separations near $f_2 = 2f_m$ for (a) $\Omega_{in} = 9000$ rpm, (b) $\Omega_{in} = 8500$ rpm, and (c) $\Omega_{in} = 7525$ rpm.

of the meshing cycle when $\Omega_{in} = 8500$ rpm while it is nearly 42% when $\Omega_{in} = 7525$ rpm. This indicates that the degree of nonlinearity is increased as one approaches the jump down frequency from the right. Other nonlinear phenomena including sub-harmonic motions and chaos were also found in earlier studies of single gear pairs [24]. The planetary gear set studied here seems to exhibit such behavior as well. For instance, near the resonance peak of $f_3 \approx 3f_m$, sub-harmonic and chaotic motions were also predicted for the same example system [25].

3.2. Influence of wear on dynamic gear mesh forces

In order to quantify the influence of surface wear on the dynamic behavior, the same baseline planetary gear set is considered now with the predicted worn profiles shown in Fig. 4. The steady state dynamic gear mesh are predicted at three levels of surface wear, $\kappa = 2$, 4 and 6, and compared to the response corresponding to the baseline case of no surface wear $\kappa = 0$.

Fig. 9 illustrates the change of $F_{s/p}^{(m)}$ time histories with κ at $\Omega_{in} = 2750$ rpm. Here $F_{s/p}^{(m)}$ changes significantly with the wear amount. Both peak-to-peak amplitudes and the shape of the waveforms are altered as κ is increased. Harmonic amplitudes of $F_{s/p}^{(m)}$ are plotted in Fig. 9(e) to show that the fundamental harmonic amplitude $i = 1$ is influenced the most by the surface wear. While $F_{s/p}^{(1)} = 13$ N per mm FW when $\kappa = 0$, it is about 30 N per mm FW when $\kappa = 6$. The higher harmonic amplitudes ($i > 1$) are increased slightly with increased κ. Because of this, the increase in the rms value $F_{s/p}^{(rms)}$ can be attributed to the increase in the fundamental harmonic. This is indeed the typical behavior observed at Ω_{in} values away from any of the resonance peaks, suggesting that the shape of the worn surface profile in off-resonance regions impacts the fundamental harmonic of the response the most.

This is not the case near the resonance peaks. Since each resonance peak is dictated by a harmonic order other than the fundamental harmonic in this case, the typical increases in $i = 1$ component with κ appears to have a secondary influence. An example of this is shown in Fig. 10 at $\Omega_{in} = 13,500$ rpm near the resonance peak at $f_3 \approx 3f_m$. In this case, while the peak-to-peak gear mesh order amplitudes increase with κ, the increase in the rms value is mostly due to the $i = 3$ harmonic component.

In Fig. 11, forced response curves of $F_{s/p}^{(rms)}$ and $F_{r/p}^{(rms)}$ for $\kappa = 2$, 4 and 6 are compared to the baseline curves ($\kappa = 0$) shown earlier in Fig. 7. One observation from these figures is that, in the off-resonance regions, $F_{s/p}^{(rms)}$ and $F_{r/p}^{(rms)}$ get consistently larger as the wear amount (κ value) is increased, primarily due to an increase in the fundamental harmonic amplitude. For instance, at $\Omega_{in} = 2000$, $F_{j/p}^{(rms)}$ values are almost doubled for $\kappa = 6$ compared to the baseline response. This suggests that both fatigue life and noise behavior of the planetary gear set away from the resonances are influenced significantly by surface wear. Similarly, a number of new resonance peaks are created with increased wear as the ones at 3000 and 7000 rpm. Meanwhile such influence does not exist at the resonance frequencies, especially when the tooth separations occur. For instance the amplitudes of upper branch motions of $f_2 \approx 2f_m$ are somewhat reduced with an increase in κ value.

Finally, $F_{r/p}^{(m)}$ time histories for $\kappa = 0$, 2, 4 and 6 are compared in Fig. 12 at $\Omega_{in} = 8000$ rpm. The baseline system ($\kappa = 0$) exhibits loss of contact of gear teeth as shown in Fig. 12(a). This loss of contact situation remains relatively unchanged as κ is increased. The nonlinear behavior dictated

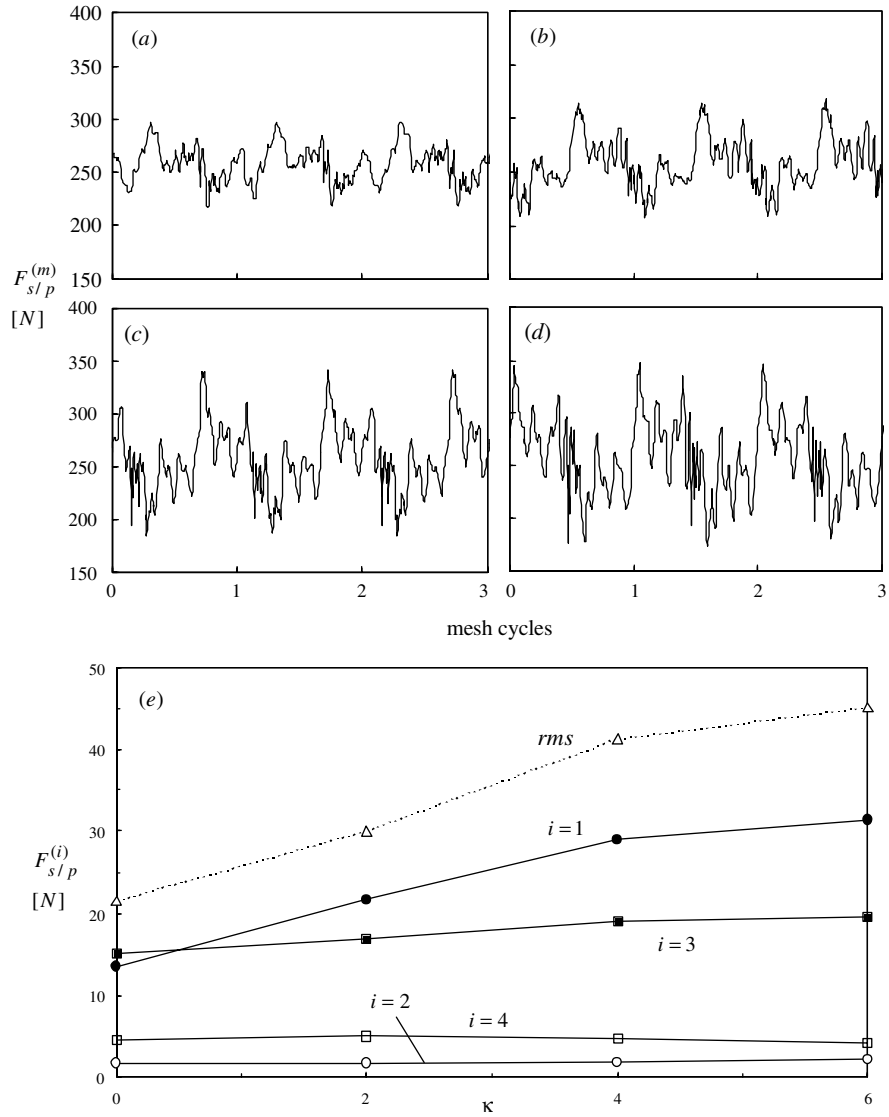

Fig. 9. $F^{(m)}_{s/p}$ time histories for (a) $\kappa = 0$, (b) $\kappa = 2$, (c) $\kappa = 4$, and (d) $\kappa = 6$ at $\Omega_{in} = 2,750$ rpm. (e) Variation of the harmonic amplitudes of $F_{s/p}$ with κ.

by the tooth separations is maintained with very little change suggesting that the surface wear has a secondary influence on the nonlinear response.

4. Conclusions

In this study, a computational model of a planetary gear set was employed to study the influence of surface wear in the dynamic behavior of a typical automotive automatic transmission

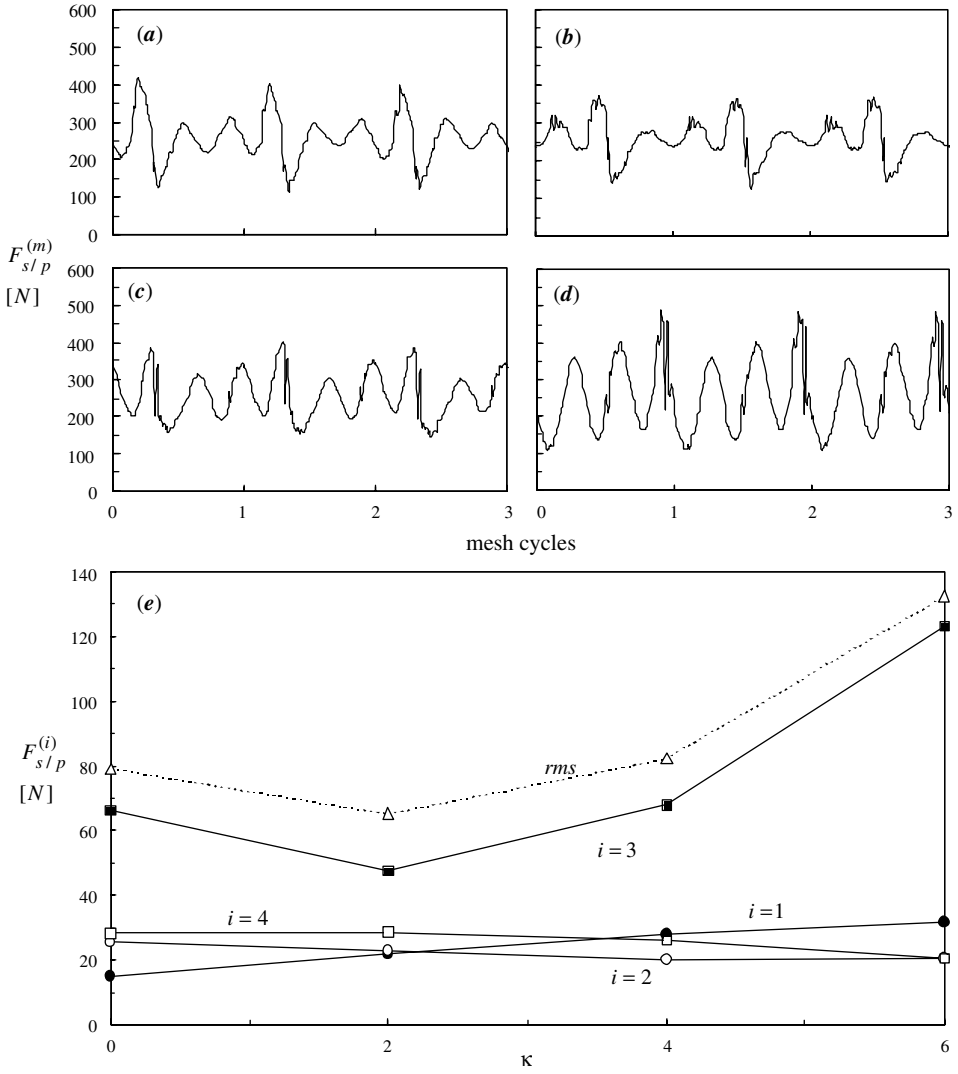

Fig. 10. $F_{s/p}^{(m)}$ time histories for (a) $\kappa = 0$, (b) $\kappa = 2$, (c) $\kappa = 4$, and (d) $\kappa = 6$ at $\Omega_{in} = 13,500$ rpm. (e) Variation of the harmonic amplitudes of $F_{s/p}$ with κ.

planetary gear set. The overall computational scheme combines a gear wear prediction model that gives geometric description of contacting tooth surfaces having wear and a deformable-body dynamic model of a planetary gear set. The wear model employs a quasi-static gear contact mechanics model to compute contact pressures and Archard's wear model to determine the wear depth distributions. The worn surfaces were input into the dynamic model to quantify the impact of wear on gear tooth and mesh dynamic forces. It was shown that a planetary gear set is inherently nonlinear, and exhibits softening type nonlinear behavior near its resonance peaks, characterized by sudden jumps of dynamic gear mesh force amplitudes. A sun gear experiences the largest amount of wear, compared to other gears in the system as the maximum wear locations are

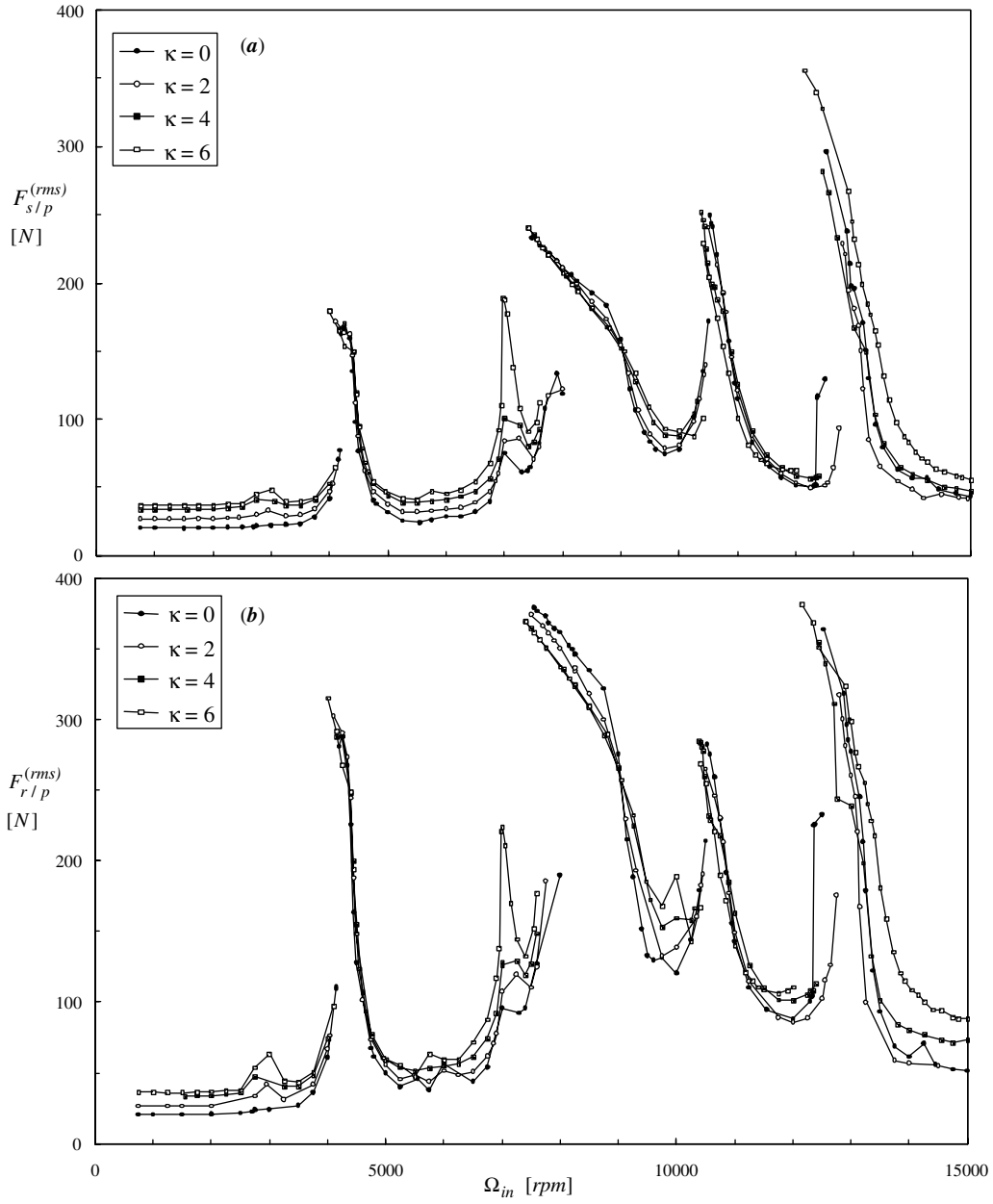

Fig. 11. Comparison of (a) $F_{s/p}^{(\mathrm{rms})}$ and (b) $F_{r/p}^{(\mathrm{rms})}$ for $\kappa = 0$, 2, 4 and 6 as a function of Ω_{in} at $T_{\mathrm{in}} = 25$ Nm/mm FW.

in the dedendum of the sun gear. It is also observed that the tooth surface wear influences the fundamental harmonic of the gear mesh forces the most. While this influence is evident in both resonance and off-resonance regions of the forced response, the impact of wear is limited in the resonance regions dictated by higher harmonics. It is also concluded that wear has a negligible

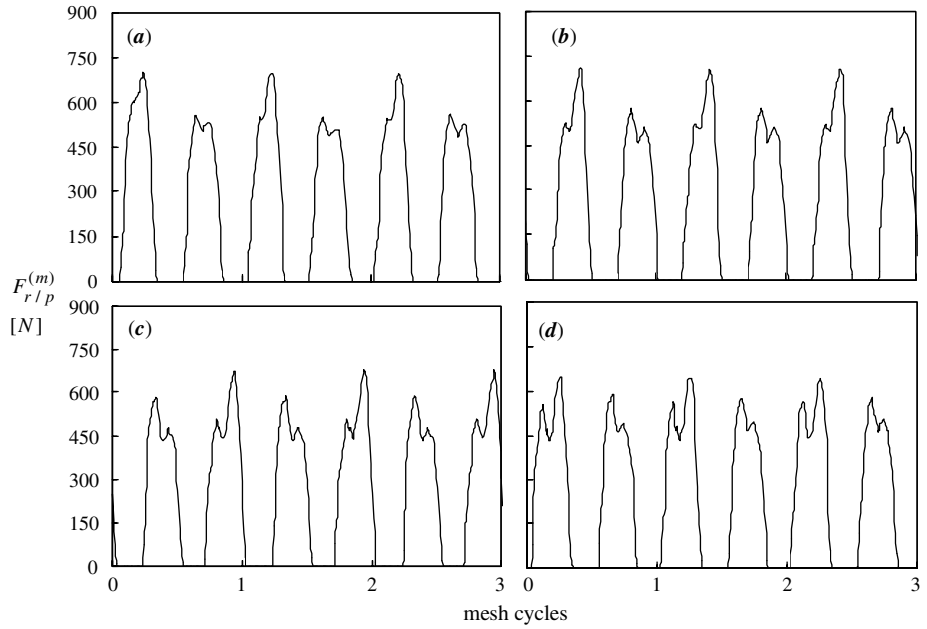

Fig. 12. Comparison of $F_{r/p}^{(m)}$ at $\Omega_{in} = 8000$ rpm near the resonance peak of $f_2 = 2f_m$ for (a) $\kappa = 0$, (b) $\kappa = 2$, (c) $\kappa = 4$, and (d) $\kappa = 6$.

influence on the nonlinear behavior as nearly the same type of tooth separations were observed with or without surface wear.

Acknowledgements

Authors thank Dr. S. Vijayakar for making the gear analysis packages CAPP and 2DPLANETARY available.

References

[1] P. Bajpai, A. Kahraman, N.E. Anderson, A surface wear prediction methodology for helical gear pairs, Transaction of ASME, Journal of Tribology 126 (2004).
[2] F. Cunliffe, J.D. Smith, D.B. Welbourn, Dynamic tooth loads in epicyclic gears, Transaction of ASME, Journal of Engineering for Industry 95 (1974) 578–584.
[3] M. Botman, Epicyclic gear vibrations, Transaction of ASME, Journal of Engineering for Industry 97 (1976) 811–815.
[4] A. Kahraman, Natural modes of planetary gear trains, Journal of Sound and Vibration 173 (1994) 125–130.
[5] J. Lin, R.G. Parker, Analytical characterization of the unique properties of planetary gear free vibration, Transaction of ASME, Journal of Vibration and Acoustics 121 (1999) 316–321.
[6] A. Kahraman, Load sharing characteristics of planetary transmissions, Mechanisms and Machine Theory 29 (1994) 1151–1165.

[7] A. Kahraman, Planetary gear train dynamics, Transaction of ASME, Journal of Mechanical Design 116 (1994) 713–720.
[8] A. Saada, P. Velex, An extended model for the analysis of the dynamic behavior of planetary trains, Transaction of ASME, Journal of Mechanical Design 117 (1995) 241–247.
[9] A. Kahraman, Free Torsional vibration characteristics of compound planetary gear sets, Mechanism and Machine Theory 36 (2001) 953–971.
[10] R.G. Parker, V. Agashe, S.M. Vijayakar, Dynamic response of a planetary gear system using a finite-element contact mechanics model, Transaction of ASME, Journal of Mechanical Design 122 (2000) 304–311.
[11] A. Kahraman, A. Kharazi, M. Umrani, A deformable-body dynamic analysis of planetary gears with thin rims, Journal of Sound and Vibration 262 (2003) 752–768.
[12] A. Kahraman, S. Vijayakar, Effect of internal gear flexibility on the quasi-static behavior of a planetary gear set, Transaction of ASME, Journal of Mechanical Design 123 (2001) 408–415.
[13] W. Shifeng, H.S. Cheng, Sliding wear calculation in spur gears, Transaction of ASME, Journal of Tribology 115 (1993) 493.
[14] A. Flodin, S. Andersson, Simulation of mild wear in spur gears, Wear 207 (1997) 16–23.
[15] A. Flodin, S. Andersson, Simulation of mild wear in helical gears, Wear 241 (2000) 123–128.
[16] A. Flodin, S. Andersson, A simplified model for wear prediction in helical gears, Wear 249 (2001) 285–292.
[17] J.F. Archard, Contact and rubbing of flat surfaces, Journal of Applied Physics 24 (1953) 981–988.
[18] J.H. Kuang, A.D. Lin, The effect of tooth wear on the vibration spectrum of a spur gear pair, Journal of Sound and Vibration 123 (2001) 311–317.
[19] F.K. Choy, V. Polyshchuk, J.J. Zakrajsek, R.F. Handschuh, D.P. Townsend, Analysis of the effects of surface pitting and wear on the vibration of a gear transmission system, Tribology International 29 (1996) 77–83.
[20] J. Wojnarowski, V. Onishchenko, Tooth wear effects on spur gear dynamics, Mechanism and Machine Theory 38 (2003) 161–178.
[21] User's Manual, CAPP, Contact Analysis Program Package, Advanced Numerical Solutions Inc., 2002.
[22] User's Manual, 2DPLANETARY, Planetary Gear Set Analysis Package, Advanced Numerical Solutions Inc., 2002.
[23] A. Kahraman, G.W. Blankenship, Planet mesh phasing in epicyclic gear sets, in: Proceedings of International Gearing Conference, Newcastle, UK, 1994, pp. 99–104.
[24] A. Kahraman, G.W. Blankenship, Steady state forced response of a mechanical oscillator with combined parametric excitation and clearance type non-linearity, Journal of Sound and Vibration 185 (1994) 734–765.
[25] C. Yuksel, Influence of surface wear on dynamic behavior of planetary gear sets, M.S. Thesis, the University of Toledo, 2003.